ISIJ International, Vol. 52 (2012), No. 3, pp. 413–423

Modeling and Validation of an Electric Arc Furnace: Part 2, Thermo-chemistry

Vito LOGAR, Dejan DOVŽAN and Igor ŠKRJANC

Laboratory of modeling, simulation and control, Faculty of Electrical Engineering, University of Ljubljana, Tržaška 25, SI-1000 Ljubljana. E-mail: vito.logar@fe.uni-lj.si, dejan.dovzan@fe.uni-lj.si, igor.skrjanc@fe.uni-lj.si

(*Received on September 2, 2011; accepted on October 11, 2011*)

The following paper presents an approach to the mathematical modeling of thermo-chemical reactions and relations in a 3–phase, 80 MVA AC, electric arc furnace (EAF) and represents a continuation of our work on modeling the electric and hydraulic processes of an EAF. This paper is part 2 of the complete EAF model and addresses the issues relating to chemical reactions and the corresponding chemical energy in the EAF, which are not included in part 1 of the paper, which is focused on mass, temperature and energy-exchange modeling. Part 2 and part 1 papers are related to each other accordingly and should be considered as a whole. The developed and presented sub-models are obtained according to mathematical and thermo-chemical laws, with the parameters fitting both experimentally, using the measured operational data of an EAF during different periods of the melting process, and theoretically, using the conclusions of different studies involved in EAF modeling. Part 2, part 1 and the already published electrical and hydraulic models of the EAF represent a complete EAF model, which can further be used for the initial aims of our project, *i.e.*, optimization of the energy consumption and the development of an operator-training simulator. Like with part 1, the obtained results show high levels of similarity with both the operational measurements and theoretical data available in different studies, from which we can conclude that the presented EAF model is developed in accordance with both the fundamental laws of thermodynamics and the practical aspects relating to EAF operation.

KEY WORDS: EAF; thermal model; chemical model; experimental validation.

1. Introduction

The paper presents an approach to the mathematical modeling of thermo-chemical processes in an 80 MVA AC, electric arc furnace (EAF). The proposed models complement the previous work on the modeling of the electrical and hydraulic processes in an EAF[1)] and the work presented in part 1, and represent the final stage of the complete EAF model. The EAF sub-models derived in this paper address the most common chemical reactions, which appear during the steel melting process and include the oxidation and reduction of both chemical elements, such as iron, carbon, silicon, manganese, chromium and phosphorus; and chemical compounds, such as iron oxide, carbon monoxide and dioxide, silica, manganese oxide, chromium oxide and phosphorus oxide. Also, the model takes into account the mechanisms of electrode oxidation, the oxidation of combustible materials, the oxygen burners, the relative pressure and the slag-foaming processes. Since the chemical reactions can contribute up to 40% of the total EAF energy balance, the model includes energy-exchange equations for each chemical reaction. For the needs of our study, the model defines relatively accurate and reliable relations that describe the chemical reactions between the EAF regions, *i.e.*, the steel, slag and gas zones.

Various approaches to the modeling of EAF chemistry and the appurtenant energy relations can be found in the literature, such as general chemical models[2,3)] or more detailed sub-processes.[4–6)] Like with the heat, temperature and mass models presented in part 1, the thermo-chemical model proposed in this paper is inspired by the papers of Bekker[2)] and MacRosty;[3)] however, the proposed model in this study is more complex, approached differently and considers more chemical reactions and additional energy transfers between the EAF zones. Also, the model includes relations describing CO post-combustion[7)] and slag-foaming processes based on the realities in the EAF and its impact on radiative heat transfer. Besides modeling the fundamental laws of mass and heat transfer, special attention is devoted to the parameterization of the developed model using available initial, endpoint and online measurements for the EAF's operation.

Like with the models developed in our previous work, the model proposed here is based on the 80 MVA AC furnace installed in one of the ironworks in Slovenia. Therefore, for the needs of a successful model parameterization, operational data of the EAF related to the chemical transfer processes were obtained, including the initial and end-point steel and slag compositions, the steel yields, the temperatures, *etc.* Since some data (the stage and rate of the chemical reactions, temperatures, masses, *etc.*) cannot be obtained during the melting, due to the nature of the process, the equations and parameters of the sub-models relating to those values

were obtained theoretically. Other measurements, such as the arc powers, which are needed to complement the proposed models, were obtained when modeling the electrical processes in the EAF.

Since the work presented in this paper complements the heat, mass and temperature models presented in part 1, a reference to part 1 is added at each necessary point as (PART 1).

2. Modeling

The following section presents the modeling approach to the thermo-chemical processes of the particular EAF. Since this paper investigates the EAF sub-models and relations that are not addressed in part 1, this paper follows the same modeling assumptions and simplifications as part 1(PART 1). Furthermore, some additional assumptions, regarding the chemical model have been made, such as:

- liquid steel is assumed to be a dilute solution, with mole fraction unit for molten steel,
- activity coefficients are assumed constant and are close to unity, with the respective reaction equilibrium constants computed accordingly,[2,4]
- the reactions are started as soon as the corresponding reactants enter the liquid form, with all other conditions met (presence of oxygen, carbon, *etc.*),
- ideal solution is assumed for slag components.

In a similar way, the EAF layout is divided into identical zones as with the previous work. The values of all the parameters used in the developed model are listed in the Appendix section. Similarly, equal notation for EAF zones is used, *i.e.*: solid scrap - *sSc*, liquid metal - *lSc*, solid slag - *sSl*, liquid slag - *lSl* and gas - *gas*.

2.1. Thermo-chemical Model

It is generally known that the chemical reactions in the steel bath, the slag and the gas zone of the EAF represent an important part of the steel-melting processes. The literature suggests that 10–40%[8] of the complete energy input is contributed by the chemical reactions, meaning that the impact of the thermo-chemical relations in the EAF cannot be neglected. Therefore, the thermo-chemical model of the EAF is important for two reasons. First, it defines the relations between the different chemical elements and compounds and influences the final composition of the steel, the slag and the off-gas. Second, the energy released from the reactions during the EAF melting process represents a significant amount of the total EAF energy balance. Newer EAF designs tend to replace more and more electrical energy with chemical energy by adding increased quantities of oxygen and carbon into the bath, which can also be taken into the account when the thermo-chemical relations are modeled properly.

The chemical model assumes that all the chemical reactions, except the CO post-combustion and CH_4 oxidation (oxygen burners) take place in the liquid metal and slag zones. The notation used is as follows: m_{xx} denotes the mass of an element or compound *xx*, M_{xx} denotes the molar mass of an element or compound *xx*, kd_{xx} represents the reaction-rate coefficient of an element *xx*, X_{xx} is the molar fraction of the element or compound *xx*, X_{xx}^{eq} is the equilibrium molar fraction of the element or compound *xx* and kX_{xx} is the equilibrium constant of the element or compound *xx*, unless specified otherwise.

Chemical reactions

The chemical reactions that are considered in the proposed model are chosen according to the influence of the particular reaction on the energy input/output to the complete EAF energy balance,[4] the chemical composition of the steel or slag and the obtained initial and end-point data of the EAF. The oxidation and reduction reactions that are taken into account are given by Eq. (1):

$$\begin{aligned}
&a)\ Fe+\frac{1}{2}O_2 \rightarrow FeO\\
&b)\ FeO+C \rightarrow Fe+CO\\
&c)\ FeO+Mn \rightarrow Fe+MnO\\
&d)\ 2FeO+Si \rightarrow 2Fe+SiO_2\\
&e)\ 3FeO+2Cr \rightarrow 3Fe+Cr_2O_3\\
&f)\ 5FeO+2P \rightarrow 5Fe+P_2O_5\\
&g)\ C+\frac{1}{2}O_2 \rightarrow CO\\
&h)\ CO+\frac{1}{2}O_2 \rightarrow CO_2\\
&i)\ C+O_2 \rightarrow CO_2\\
&j)\ MnO+C \rightarrow Mn+CO\\
&k)\ 2MnO+Si \rightarrow 2Mn+SiO_2\\
&l)\ Si+O_2 \rightarrow SiO_2\\
&m)\ 2Cr+\frac{3}{2}O_2 \rightarrow Cr_2O_3\\
&n)\ CH_4+2O_2 \rightarrow CO_2+2H_2O\\
&p)\ C_9H_{20}+54O_2 \rightarrow 9CO_2+90H_2O
\end{aligned} \quad \text{..... (1)}$$

The above reactions represent the basis for the development of the model, *i.e.*, computing the rates of change of the elements or compounds and the input or output energies of a particular reaction. The details of the proposed reactions are presented below. At this point the number of moles of liquid metal (XM_{lSc}) and slag (XM_{lsl}) zones shall be defined in Eq. (2), as they are frequently used later.

$$\begin{aligned}
XM_{lSc} &= \frac{m_{lSc}}{M_{Fe}}+\frac{m_C}{M_C}+\frac{m_{Si}}{M_{Si}}+\frac{m_{Cr}}{M_{Cr}}+\frac{m_{Mn}}{M_{Mn}}+\frac{m_P}{M_P}\\
XM_{lSl} &= \frac{m_{lSl}}{M_{lSl}}+\frac{m_{FeO}}{M_{FeO}}+\frac{m_{SiO2}}{M_{SiO2}}+\frac{m_{MnO}}{M_{MnO}}+\frac{m_{Cr2O3}}{M_{Cr2O3}}+\frac{m_{P2O5}}{M_{P2O5}}
\end{aligned} \quad \text{..... (2)}$$

The molar fraction of an element X_{xx} or compound X_{yy}, where *xx* denotes the particular element and *yy* the compound can be defined in a uniform way by Eqs. (3) and (4). The model assumes that all the elements *xx* are present (dissolved) in the liquid metal, while the compounds *yy* are present in the liquid slag (except the gases).

$$X_{xx}=\frac{m_{xx}/M_{xx}}{XM_{lSc}} \quad \text{..... (3)}$$

$$X_{yy}=\frac{m_{yy}/M_{yy}}{XM_{lSl}} \quad \text{..... (4)}$$

Rate of change of carbon (C)

The rate of change of carbon in the bath ($\dot{m}_{C-L}$ and $\dot{m}_{C-D}$) is determined by the following mechanisms: C injection ($x1_{d1}$), injected C decarburization ($x1_{d2}$) [Eq. (1b)], injected C dissolving ($x1_{d3}$), dissolved C decarburization ($x2_{d1}$) [Eq. (1b)], dissolved C oxidation to CO ($x2_{d2}$) [Eq. (1g)], dissolved C increase due to dissolving of the injected C ($x2_{d3}$), reaction with MnO ($x2_{d4}$) [Eq. (1j)] and dissolved C oxidation to CO_2 ($x2_{d5}$) [Eq. (1i)]. The rate of change of injected C ($\dot{m}_{C-L}$) is given by Eq. (5):

$$\begin{aligned} x1_{d1} &= C_{inj} \\ x1_{d2} &= -\frac{m_{FeO} kd_{C-L} m_{C-L}}{m_{lSl} + m_{FeO} + m_{SiO2} + m_{MnO} + m_{Cr2O3} + m_{P2O5}} \\ x1_{d3} &= -\frac{m_{C-L} T_{lSc} C_{p,lSc} \frac{T_{air}}{T_{melt}}}{\lambda_C + C_{p,C}(T_{melt} - T_{air})} \\ \dot{m}_{C-L} &= \sum_{i=1}^{3} x1_{di}, \end{aligned} \quad \text{... (5)}$$

where C_{inj} is the carbon injection rate (kg/s), $kd_{C\text{-}L}$ is the decarburization rate and $m_{C\text{-}L}$ is the mass of injected carbon present in the furnace.

The rate of change of the dissolved C in the bath ($\dot{m}_{C-D}$) is given by Eq. (6):

$$\begin{aligned} x2_{d1} &= -kd_{C-D}(X_C - X_C^{eq}) \\ x2_{d2} &= -kd_{C-1}(X_C - X_C^{eq}) O2_{lance} \cdot K_{O2-CO} \\ x2_{d3} &= -x1_{d3} \\ x2_{d4} &= -kd_{Mn-1} \frac{M_C}{M_{MnO}} (X_{MnO} - X_{MnO-1}^{eq}) \\ x2_{d5} &= -kd_{C-2}(X_C - X_C^{eq}) O2_{lance} \cdot K_{O2-CO2} \\ \dot{m}_{C-D} &= \sum_{i=1}^{5} x2_{di}, \end{aligned} \quad \text{..... (6)}$$

where $kd_{C\text{-}D}$ is the FeO decarburization rate, $kd_{C\text{-}1}$ is the C oxidation rate to CO, $kd_{Mn\text{-}1}$ is the MnO decarburization rate, $kd_{C\text{-}2}$ is the C oxidation rate to CO_2, $O2_{lance}$ is the oxygen lance rate, $K_{O2\text{-}CO}$ and $K_{O2\text{-}CO2}$ are the fractions of the lanced oxygen used for oxidizing C to CO and CO_2, respectively.

The molar fractions of FeO, MnO and C (X_{FeO}, X_{MnO} and X_C) needed in Eq. (6) are obtained with Eqs. (3) and (4); the equilibrium molar fraction of C in the bath is defined similarly as proposed by Bekker;[2] but in an extended form and is obtainable with Eq. (7):

$$X_C^{eq} = \frac{kX_C}{X_{FeO}}, \quad \text{..... (7)}$$

where kX_C is the reaction equilibrium constant for the FeO + C reaction [Eq. (1b)] defined as $kX_C = 4.9\times10^{-4}$ and is obtainable with Eq. (8):

$$\begin{aligned} k_{C\%} &= X_{FeO} X_C \left(\frac{M_{FeO} M_C}{M_{lSl} M_{Fe}} 100^2 \right) = 1.25 \\ kX_C &= X_{FeO} X_C = k_{C\%} \frac{1}{X_{FeO}}. \end{aligned} \quad \text{..... (8)}$$

As suggested by Ref. 4) the equilibrium molar fraction of MnO used in Eq. (6) can be described with Eq. (9):

$$X_{MnO-1}^{eq} = \frac{X_{Mn}}{kX_{Mn-1}}, \quad \text{..... (9)}$$

where $kX_{Mn\text{-}1}$ is the reaction equilibrium constant for the MnO + C reaction [Eq. (1j)], defined by Eq. (10):[4]

$$\begin{aligned} k_{Mn-1\%} &= p_{CO} \frac{X_{Mn}}{X_{MnO-1}} \frac{M_{Fe} M_{MnO}}{M_{Mn} M_{lSl}} = 6.4 p_{CO} \\ kX_{Mn-1} &= \frac{X_{Mn}}{X_{MnO-1}} = k_{Mn-1\%} X_{MnO-1}, \end{aligned} \quad \text{..... (10)}$$

where p_{CO} represents the partial pressure of CO.

Rate of change of silicon (Si)

The rate of change of dissolved silicon in the bath ($\dot{m}_{Si}$) is determined by the following mechanisms: Si desiliconization ($x3_{d1}$) [Eq. (1d)], Si oxidation to SiO_2 ($x3_{d2}$) [Eq. (1l)] and Si reaction with MnO ($x3_{d3}$) [Eq. (1k)]. The rate of change of dissolved Si can be obtained with Eq. (11):

$$\begin{aligned} x3_{d1} &= -kd_{Si-1}(X_{Si} - X_{Si}^{eq}) \\ x3_{d2} &= -kd_{Si-2}(X_{Si} - X_{Si}^{eq}) O2_{lance} \cdot K_{O2-SiO2} \\ x3_{d3} &= -kd_{Mn-2} \frac{M_{Si}}{M_{MnO}} (X_{MnO} - X_{MnO-2}^{eq}) \\ \dot{m}_{Si} &= \sum_{i=1}^{3} x3_{di}, \end{aligned} \quad \text{.....(11)}$$

where $kd_{Si\text{-}1}$ is the FeO desiliconization rate, $kd_{Si\text{-}2}$ is the Si oxidation rate to SiO_2, $kd_{Si\text{-}3}$ is the MnO desiliconization rate and $K_{O2\text{-}SiO2}$ is the fraction of the lanced oxygen used for oxidizing Si to SiO_2.

The molar fractions of FeO, MnO and Si are obtainable with Eqs. (3) and (4); the equilibrium molar fraction of Si in the bath is defined like in;[2] but in an extended form and is obtainable with Eq. (12):

$$X_{Si}^{eq} = \frac{kX_{Si}}{X_{FeO}^2}, \quad \text{..... (12)}$$

where kX_{Si} is the dimensionless reaction equilibrium constant for the FeO + Si reaction [Eq. (1d)] defined as $kX_{Si} = 8.08\times10^{-8}$ and is obtainable with Eq. (13):

$$\begin{aligned} k_{Si\%} &= X_{FeO}^2 X_{Si} \left(\frac{M_{FeO}^2 M_{Si}}{M_{lSl}^2 M_{Fe}} 100^3 \right) = 5.7 \cdot 10^{-4} \\ kX_{Si} &= X_{FeO}^2 X_{Si} = k_{Si\%} \left(\frac{M_{lSl}^2 M_{Fe}}{M_{FeO}^2 M_{Si} 100^3} \right). \end{aligned} \quad \text{..... (13)}$$

As suggested by Ref. 4) the equilibrium molar fraction of MnO can be, for the particular reaction, described by Eq. (14):

$$X_{MnO-2}^{eq} = \sqrt{\frac{X_{Mn}^2 X_{SiO2}}{X_{Si} kX_{Mn-2}}}, \quad \text{..... (14)}$$

where $kX_{Mn\text{-}2}$ is the dimensionless reaction-equilibrium constant for the MnO + Si reaction [Eq. (1k)], defined by Eq. (15):

$$kX_{Mn-2} = 10^{2.8 \frac{X_{CaO} + X_{MgO}}{X_{SiO2}} - 1.16} \frac{M_{MnO}^2 M_{Si} M_{Fe}}{M_{Mn}^2 M_{lSl} M_{SiO2}}. \quad \text{..... (15)}$$

Rate of change of Manganese (Mn)

The rate of change of dissolved manganese in the bath ($\dot{m}_{Mn}$) is determined by the following mechanisms: the Mn reaction with FeO ($x4_{d1}$) [Eq. (1c)], the MnO reaction with C ($x4_{d2}$) [Eq. (1j)] and the MnO reaction with Si ($x4_{d3}$) [Eq. (1k)]. The rate of change of dissolved Mn can be obtained with Eq. (16):

$$\begin{aligned} x4_{d1} &= -kd_{Mn}(X_{Mn} - X_{Mn}^{eq}) \\ x4_{d2} &= -\frac{M_{Mn}}{M_C} x2_{d4} \\ x4_{d3} &= -\frac{M_{Mn}}{M_{Si}} x3_{d3} \\ \dot{m}_{Mn} &= \sum_{i=1}^{3} x4_{di}, \end{aligned} \quad \text{..... (16)}$$

where kd_{Mn} is the rate of the FeO + Mn reaction. The molar fraction of Mn is obtainable with Eq. (3), while the equilibrium molar fraction of Mn in the bath is obtainable with Eq. (17):

$$X_{Mn}^{eq} = \frac{X_{MnO}}{X_{FeO} kX_{Mn}}, \quad \text{..... (17)}$$

where kX_{Mn} is the dimensionless reaction equilibrium constant for the reaction [Eq. (1c)] defined as kX_{Mn} = 189.3 and is obtained from the Eq. (18):[4]

$$\begin{aligned} k_{Mn\%} &= \frac{X_{MnO}}{X_{FeO} X_{Mn}} \left(\frac{M_{MnO} M_{Fe}}{M_{FeO} M_{Mn} 100} \right) = 1.9 \pm 0.3 \\ kX_{Mn} &= \frac{X_{MnO}}{X_{FeO} X_{Mn}} = k_{Mn\%} \frac{M_{FeO} M_{Mn} 100}{M_{MnO} M_{Fe}}. \end{aligned} \quad \text{.... (18)}$$

Rate of change of chromium (Cr)

The rate of change of dissolved chromium in the bath ($\dot{m}_{Cr}$) is determined with the following mechanisms: the Cr reaction with FeO ($x5_{d1}$) [Eq. (1e)] and Cr oxidation ($x5_{d2}$) [Eq. (1m)]. The rate of change of dissolved Cr can be obtained with Eq. (19):

$$\begin{aligned} x5_{d1} &= -2kd_{Cr-1}(X_{Cr} - X_{Cr}^{eq}) \\ x5_{d2} &= -4kd_{Cr-2}(X_{Cr} - X_{Cr}^{eq}) O2_{lance} \cdot K_{O2-Cr2O3} \\ \dot{m}_{Cr} &= \sum_{i=1}^{2} x5_{di}, \end{aligned} \quad \text{... (19)}$$

where $kd_{Cr\text{-}1}$, $kd_{Cr\text{-}2}$ are the reaction rates and $K_{O2\text{-}Cr2O3}$ is the fraction of the lanced oxygen used for oxidizing Cr to Cr_2O_3. The molar fraction of Cr is obtainable with Eq. (3), while the equilibrium molar fraction of Cr in the bath is obtainable with Eq. (20):

$$X_{Cr}^{eq} = \frac{X_{Cr2O3}}{X_{FeO} kX_{Cr}}, \quad \text{..... (20)}$$

where kX_{Cr} is the dimensionless reaction-equilibrium constant for the chromium defined as kX_{Cr} = 13.2 and is obtained from the Eq. (21):[4]

$$\begin{aligned} k_{Cr\%} &= \frac{X_{Cr2O3}}{X_{Cr} X_{FeO}} \left(\frac{M_{Cr2O3} M_{Fe}}{M_{Cr} M_{FeO} 100} \right) = 0.3 \pm 0.1 \\ kX_{Cr} &= \frac{X_{Cr2O3}}{X_{Cr} X_{FeO}} = k_{Cr\%} \frac{M_{Cr} M_{FeO} 100}{M_{Cr2O3} M_{Fe}}. \end{aligned} \quad \text{..... (21)}$$

Rate of change of phosphorus (P)

The rate of change of dissolved phosphorus in the bath ($\dot{m}_P$) is determined with the following mechanism: P oxidation ($x6_{d1}$) [Eq. (1f)]. The rate of change of dissolved P can be obtained with Eq. (22):

$$\begin{aligned} x6_{d1} &= -2kd_P(X_P - X_P^{eq}) \\ \dot{m}_P &= x6_{d1}, \end{aligned} \quad \text{..... (22)}$$

where kd_P is the rate of reaction. The molar fraction of P is obtainable with Eq. (3), while the equilibrium molar fraction of P in the bath is obtainable with Eq. (23):

$$X_P^{eq} = \sqrt{\frac{X_{P2O5}}{X_{FeO}^5 X_{CaO}^3 kX_P}}, \quad \text{..... (23)}$$

where kX_P is the dimensionless reaction-equilibrium constant for phosphorus defined as $kX_P = 7.8 \times 10^3$ and is obtained from the Eq. (24):[9]

$$\begin{aligned} k_{P\%} &= \frac{X_{P2O5}}{X_P^2 X_{FeO}^5 X_{CaO}^3} \left(\frac{M_{P2O5} M_{Fe}^2 M_{lSl}^7}{M_P^2 M_{FeO}^5 M_{CaO}^3 100^9} \right) = 9.8 \cdot 10^{-4} \\ kX_P &= \frac{X_{P2O5}}{X_P^2 X_{FeO}} = k_{Cr\%} \frac{M_{Cr} M_{FeO} 100}{M_{Cr2O3} M_{Fe}}. \end{aligned} \quad \text{.. (24)}$$

Rate of change of iron oxide (FeO)

The rate of change of the iron oxide in the slag ($\dot{m}_{FeO}$) is determined by the following mechanism: injected C decarburization $x7_{d1}$ [Eq. (1b)], Si desiliconization $x7_{d2}$ [Eq. (1d)], Fe oxidation $x7_{d3}$ [Eq. (1a)], FeO added by DRI $x7_{d4}$, dissolved C decarburization $x7_{d5}$ [Eq. (1b)], reaction with Cr $x7_{d6}$ [Eq. (1e)], reaction with Mn $x7_{d7}$ [Eq. (1c)], reaction with P $x7_{d8}$ [Eq. (1f)]. The rate of change of FeO in the slag can be obtained with Eq. (25):

$$\begin{aligned} x7_{d1} &= \frac{M_{FeO}}{M_C} x1_{d2} \\ x7_{d2} &= 2\frac{M_{FeO}}{M_{Si}} x3_{d1} \\ x7_{d3} &= 2\frac{M_{FeO}}{M_{O2}} O2_{lance} \cdot K_{O2-FeO} \\ x7_{d4} &= DRI_{add} \cdot K_{FeO-DRI} \\ x7_{d5} &= \frac{M_{FeO}}{M_C} x2_{d1} \\ x7_{d6} &= \frac{3M_{FeO}}{2M_{Cr}} x5_{d1} \\ x7_{d7} &= \frac{M_{FeO}}{M_{Mn}} x4_{d1} \\ x7_{d8} &= \frac{5M_{FeO}}{2M_P} x6_{d1} \\ \dot{m}_{FeO} &= \sum_{i=1}^{8} x7_{di}, \end{aligned} \quad \text{..... (25)}$$

where $K_{O2\text{-}FeO}$ is the fraction of the lanced oxygen used for oxidizing Fe to FeO, DRI_{add} is the DRI addition rate and $K_{FeO\text{-}DRI}$ is the amount of FeO in the DRI stream.

Rate of change of silica (SiO_2)

The rate of change of silicon oxide in the slag ($\dot{m}_{SiO2}$) is determined by the following mechanism: Si desiliconization [Eq. (1d)], Si oxidation to SiO_2 [Eq. (1l)] and Si reaction with MnO [Eq. (1k)]. As it is clear from Eq. (11), all three equations with Si either produce or consume SiO_2. Therefore, the rate of change of SiO_2 in the slag is proportional to the rate of change of Si in the metal, and can be obtained with Eq. (26):

$$\dot{m}_{SiO2} = -\frac{M_{SiO2}}{M_{Si}} \dot{m}_{Si} \cdot \quad \text{..... (26)}$$

Rate of change of manganese oxide (MnO)

The rate of change of the manganese oxide in the slag ($\dot{m}_{MnO}$) is determined with the following mechanism: the Mn reaction with FeO [Eq. (1c)], the MnO reaction with C [Eq. (1j)] and the MnO reaction with Si [Eq. (1k)]. As is clear from Eq. (16), all three equations with Mn either produce or consume MnO. Therefore, the rate of change of the MnO in the slag is proportional to the rate of change of Mn in the metal, and can be obtained with Eq. (27):

$$\dot{m}_{MnO} = -\frac{M_{MnO}}{M_{Mn}} \dot{m}_{Mn} \cdot \quad \text{..... (27)}$$

Rate of change of chromium oxide (Cr_2O_3)

The rate of change of chromium oxide in the slag ($\dot{m}_{Cr2O3}$) is determined by the following mechanism: the Cr reaction with FeO [Eq. (1e)] and Cr oxidation [Eq. (1m)]. Like with the SiO_2 and MnO reaction mechanisms, Eq. (19) shows that both reactions with Cr produce Cr_2O_3. Therefore, the rate of change of Cr_2O_3 in the slag is proportional to the rate of change of Cr in the metal, and can be obtained with Eq. (28):

$$\dot{m}_{Cr2O3} = -\frac{M_{Cr2O3}}{2M_{Cr}} \dot{m}_{Cr} \cdot \quad \text{..... (28)}$$

Rate of change of phosphorus oxide (P_2O_5)

The rate of change of phosphorus oxide in the slag ($\dot{m}_{P2O5}$) is determined using one mechanism, *i.e.*, P oxidation [Eq. (1f)], and is proportional to the rate of change of P and can be obtained with Eq. (29):

$$\dot{m}_{P2O5} = -\frac{M_{P2O5}}{2M_P} \dot{m}_P \cdot \quad \text{..... (29)}$$

Rate of change of iron (Fe)

All the reactions that include Fe, influence its overall mass in the bath. Therefore, the rate of change of iron in the bath ($\dot{m}_{Fe}$) is determined by the following mechanism: injected C decarburization ($x8_{d1}$) [Eq. (1b)], Si desiliconization ($x8_{d2}$) [Eq. (1d)], Fe oxidation ($x8_{d3}$) [Eq. (1a)], Fe added by the DRI stream ($x8_{d4}$), dissolved C decarburization ($x8_{d5}$) [Eq. (1b)], FeO reaction with Cr ($x8_{d6}$) [Eq. (1e)], FeO reaction with Mn ($x8_{d7}$) [Eq. (1c)] and FeO reaction with P ($x8_{d8}$) [Eq. (1f)]. The rate of change of Fe in the bath can be obtained with Eq. (30):

$$\begin{aligned}
x8_{d1} &= -\frac{M_{Fe}}{M_C} x1_{d2} \\
x8_{d2} &= -2\frac{M_{Fe}}{M_{Si}} x3_{d1} \\
x8_{d3} &= -\frac{M_{Fe}}{M_{FeO}} x7_{d3} \\
x8_{d4} &= DRI_{add} \cdot K_{Fe-DRI} \\
x8_{d5} &= -\frac{M_{Fe}}{M_C} x2_{d1} \\
x8_{d6} &= -\frac{3M_{Fe}}{2M_{Cr}} x5_{d1} \\
x8_{d7} &= -\frac{M_{Fe}}{M_{Mn}} x4_{d1} \\
x8_{d8} &= -\frac{5M_{Fe}}{2M_P} x6_{d1} \\
\dot{m}_{Fe} &= \sum_{i=1}^{9} x8_{di},
\end{aligned} \quad \text{..... (30)}$$

where DRI_{add} is the DRI addition rate and $K_{Fe\text{-}DRI}$ is the amount of Fe in the DRI stream. The overall mass of Fe is obtained with Eq. (44) in part 1[(PART 1)].

Rate of change of carbon monoxide (CO)

The rate of change of carbon monoxide in the gas zone ($\dot{m}_{CO}$) is determined by the following mechanisms: CO extraction through the off-gas vents ($x9_{d1}$), CO as a product of oxidation ($x9_{d2}$) [Eq. (1g)], CO combustion with leak air ($x9_{d3}$) [Eq. (1h)], CO extraction through the hatches ($x9_{d4}$) and CO post-combustion ($x9_{d5}$) [Eq. (1h)]. CO rates $x9_{d1}$, $x9_{d3}$ and $x9_{d4}$ are defined in a similar way as proposed by Bekker,[2)] but in an extended form, while other rates are added to satisfy the needs of the proposed model. The rate of change of CO in the gas can be obtained with Eq. (31):

$$\begin{aligned}
x9_{d1} &= -\frac{h_d u_1 m_{CO}}{(k_U u_2 + h_d)(m_{CO} + m_{CO2} + m_{N2} + m_{O2})} \\
x9_{d2} &= -\frac{M_{CO}}{M_C}(x1_{d2} + x2_{d1} + x2_{d2} + x2_{d4}) \\
x9_{d3} &= 2M_{CO} k_{AIR1} k_{PR} r_P \\
x9_{d4} &= -\frac{k_{PR} r_P m_{CO}}{m_{CO} + m_{CO2} + m_{N2} + m_{O2}} \\
x9_{d5} &= -2\frac{M_{CO}}{M_{O2}} O2_{post} K_{mCO} \\
&if\ (r_P>0)\ then\ \dot{m}_{CO} = \sum_{i=1}^{5} x9_{di} - x9_{d3} \\
&if\ (r_P<0)\ then\ \dot{m}_{CO} = \sum_{i=1}^{5} x9_{di} - x9_{d4}
\end{aligned} \quad \text{.. (31)}$$

where h_d is the characteristic dimension of the duct area at the slip gap, u_1 is an approximation of the off-gas mass flow, k_U is a dimensionless constant used for improving the approximation, set to the same value as proposed by Ref. 2), u_2 is the slip-gap width, k_{AIR1} is the molar amount of O_2 in the leak air, k_{PR} represents the dimensionless constant, which defines the ratio between the reaction rate and relative

pressure,[2] r_P is the relative pressure in the EAF (Eq. (35)), $O2_{post}$ is the oxygen rate for CO post-combustion and K_{mCO} is the coefficient of CO mass [0–1], which denotes whether there is enough CO in the gas zone for post-combustion.

Rate of change of carbon dioxide (CO_2)

The rate of change of carbon dioxide in the gas zone ($\dot{m}_{CO2}$) is determined with the following mechanisms: CO_2 extraction through the off-gas vents ($x10_{d1}$), CO_2 as a product of CO combustion with leak air ($x10_{d2}$) [Eq. (1h)], CO post-combustion ($x10_{d3}$) [Eq. (1h)], CO_2 as a product of oxygen burners ($x10_{d4}$) [Eq. (1n)], electrode oxidation ($x10_{d5}$) [Eq. (1i)], oxidation of the combustible materials ($x10_{d6}$) [Eq. (1p)], CO_2 extraction through the hatches ($x10_{d7}$) and direct C oxidation to CO_2 ($x10_{d8}$) [Eq. (1i)]. The rate of change of CO_2 in the gas can be obtained with Eq. (32):

$$
\begin{aligned}
x10_{d1} &= -\frac{h_d u_1 m_{CO2}}{(k_U u_2 + h_d)(m_{CO} + m_{CO2} + m_{N2} + m_{O2})} \\
x10_{d2} &= 2M_{CO2} k_{AIR1} k_{PR} r_P \\
x10_{d3} &= 2\frac{M_{CO2}}{M_{O2}} O2_{post} K_{mCO} \\
x10_{d4} &= \frac{M_{CO2}}{M_{CH4}} CH4_{inj} \\
x10_{d5} &= \frac{M_{CO2}}{M_C} \dot{m}_{el} \\
x10_{d6} &= -9\frac{M_{CO2}}{M_{C9H_{20}}} \dot{m}_{comb} \\
x10_{d7} &= -\frac{k_{PR} r_P m_{CO2}}{m_{CO} + m_{CO2} + m_{N2} + m_{O2}} \\
x10_{d8} &= -\frac{M_{CO2}}{M_C} x2_{d5} \\
&if\ (r_P>0)\ then\ \dot{m}_{CO2} = \sum_{i=1}^{8} x10_{di} - x10_{d2} \\
&if\ (r_P<0)\ then\ \dot{m}_{CO2} = \sum_{i=1}^{8} x10_{di} - x10_{d7}.
\end{aligned}
\qquad \text{..... (32)}
$$

Rate of change of nitrogen (N_2)

The rate of change of nitrogen in the gas zone ($\dot{m}_{N2}$) is determined by the following mechanisms: N_2 extraction through the off-gas vents ($x11_{d1}$), N_2 sucked in leak air ($x11_{d2}$) and N_2 extraction through the hatches ($x11_{d3}$). The rate of change of N_2 in the gas can be obtained with Eq. (33):

$$
\begin{aligned}
x11_{d1} &= -\frac{h_d u_1 m_{N2}}{(k_U u_2 + h_d)(m_{CO} + m_{CO2} + m_{N2} + m_{O2})} \\
x11_{d2} &= -M_{N2} k_{AIR2} k_{PR} r_P \\
x11_{d3} &= -\frac{k_{PR} r_P m_{N2}}{m_{CO} + m_{CO2} + m_{N2} + m_{O2}} \\
&if\ (r_P > 0)\ then\ \dot{m}_{N2} = \sum_{i=1}^{3} x11_{di} - x11_{d2} \\
&if\ (r_P<0)\ then\ \dot{m}_{N2} = \sum_{i=1}^{3} x11_{di} - x11_{d3},
\end{aligned}
\qquad \text{..... (33)}
$$

where k_{AIR2} is the molar amount of N_2 in leak air.

Rate of change of oxygen (O_2)

The rate of change of oxygen in the gas zone ($\dot{m}_{O2}$) is determined by the following mechanisms: O_2 extraction through the off-gas vents ($x12_{d1}$), O_2 sucked in leak air ($x12_{d2}$), CO leak-air combustion ($x12_{d3}$) [Eq. (1h)], CO post-combustion ($x12_{d4}$) [Eq. (1h)], electrode oxidation ($x12_{d5}$) [Eq. (1i)], oxidation of the combustible materials ($x12_{d6}$) [Eq. (1p)], O_2 extraction through the hatches ($x12_{d7}$) and direct Fe oxidation to FeO ($x12_{d8}$) [Eq. (1a)]. The rate of change of O_2 in the gas can be obtained with Eq. (34):

$$
\begin{aligned}
x12_{d1} &= -\frac{h_d u_1 m_{O2}}{(k_U u_2 + h_d)(m_{CO} + m_{CO2} + m_{N2} + m_{O2})} \\
x12_{d2} &= -M_{O2} k_{AIR1} k_{PR} r_P \\
x12_{d3} &= -\frac{M_{O2}}{2M_{CO2}} x10_{d2} \\
x12_{d4} &= O2_{post}(1 - K_{mCO}) \\
x12_{d5} &= -\frac{M_{O2}}{M_C} \dot{m}_{el} \\
x12_{d6} &= -14\frac{M_{O2}}{M_{C9H_{20}}} \dot{m}_{comb} \\
x12_{d7} &= -\frac{k_{PR} r_P m_{O2}}{m_{CO} + m_{CO2} + m_{N2} + m_{O2}} \\
x12_{d8} &= -\frac{M_{O2}}{M_{FeO}} x7_{d3} \\
&if\ (r_P>0)\ then\ \dot{m}_{O2} = \sum_{i=1}^{8} x12_{di} - x12_{d2} \\
&if\ (r_P<0)\ then\ \dot{m}_{O2} = \sum_{i=1}^{8} x12_{di} - x12_{d7}.
\end{aligned}
\qquad \text{..... (34)}
$$

When the amount of O_2 in the gas phase is insufficient to carry out all the oxidation processes, the model decreases the amount of available O_2 for those reactions accordingly.

2.2. Relative Pressure

The relative pressure in the EAF gas zone changes as a consequence of the gases produced in the chemical reactions, off-gas vents, carbon and oxygen addition, *etc.*, and as a consequence of the temperature change. The pressure in the furnace can be obtained by following the ideal gas equation, which yields Eq. (35):

$$
\begin{aligned}
r_P = &\frac{R_{gas} T_{gas}}{V_{gas}} \left(\frac{\dot{m}_{CO}}{M_{CO}} + \frac{\dot{m}_{CO2}}{M_{CO2}} + \frac{\dot{m}_{N2}}{M_{N2}} + \frac{\dot{m}_{O2}}{M_{O2}} \right) \\
&+ \frac{R_{gas} \dot{T}_{gas}}{V_{gas}} \left(\frac{m_{CO}}{M_{CO}} + \frac{m_{CO2}}{M_{CO2}} + \frac{m_{N2}}{M_{N2}} + \frac{m_{O2}}{M_{O2}} \right),
\end{aligned}
\qquad \text{.... (35)}
$$

where R_{gas} represents the gas constant and V_{gas} represents the volume of the gas zone. The first part of Eq. (35) accounts for the pressure change due to the change of the gas masses and the second part for the change in the temperature of the gas zone.

2.3. Electrode Oxidation and Combustible Materials

As is generally known, while operating an EAF the

graphite electrodes are oxidized, which also represents a minor source of energy, which has to be added to the total EAF energy balance. According to Bowman,[5] the consumption of the electrodes ($\dot{m}_{el}$) can be described by the following Eq. (36):

$$\dot{m}_{el} = 3\left(R_{tip} \frac{I_{arc}^2}{3600} + R_{side} \frac{A_{side}}{3600} \right), \quad \text{..... (36)}$$

where R_{tip} and R_{side} are the average oxidation rates for the electrode tip ([kg/kA per h]) and side ([kg/m^2 per h]), I_{arc} represents the arc current and A_{side} represents the electrode side surface area.

A minor source of energy can also be found in the combustible materials present in the solid scrap, such as oil, grease, coatings, colors *etc.* These materials burn very quickly at the beginning of the melting process, when the temperature of the scrap is sufficiently high. The rate of change of the combustible materials ($\dot{m}_{comb}$) can be defined with Eq. (37):

$$\dot{m}_{comb} = -kd_{comb} m_{comb} \frac{T_{sSc}}{T_{melt}}, \quad \text{..... (37)}$$

where kd_{comb} is the combustion rate and $\frac{T_{sSc}}{T_{melt}}$ represents the increasing rate of combustion with the increasing temperature of the solid steel.

2.4. Energy of Chemical Reactions

With the chemical reactions and mass transfers of the elements defined, the energies of the chemical reactions can be computed. In general, the enthalpy of a reaction can be obtained with Eq. (38):[4]

$$\Delta H_T^\circ = \sum \Delta H_{298}^\circ(products) - \sum \Delta H_{298}^\circ(reactants) + \int_{298}^{T} \left[\sum C_p(products) - \sum C_p(reactants) \right] dT, \quad \text{... (38)}$$

meaning that the change of the enthalpy accompanying the given reaction is given by the difference between the enthalpies of the products and those of the reactants and by the temperature integral (from the initial (298 K) to the actual temperature) of the difference between the specific heat capacities of the products and the reactants. Using the actual variables and reactions presented here, the change of the enthalpies can be obtained from Eqs. (39) to (52), where the suffixes *-a* to *-n* in ΔH_T° denote the associated reaction from Eq. (1) in Section 2.1:

$$\Delta H_{T-a}^\circ = \frac{x8_{d3}}{M_{Fe}} \left((\Delta H_{FeO} - \Delta H_{Fe-S}) + \int_{298}^{T_{lSc}} (C_{p,FeO} - C_{p,Fe} - 0.5C_{p,O2}) dT \right) \quad \text{..... (39)}$$

$$\Delta H_{T-b}^\circ = \frac{x1_{d2} + x2_{d2}}{M_C} \left((\Delta H_{CO} - \Delta H_{C-S} - \Delta H_{FeO}) + \int_{298}^{T_{lSc}} (C_{p,Fe} + C_{p,CO} - C_{p,C} - C_{p,FeO}) dT \right) \quad \text{..... (40)}$$

$$\Delta H_{T-c}^\circ = \frac{x4_{d1}}{M_{Mn}} \left((\Delta H_{MnO} - \Delta H_{FeO} - \Delta H_{Mn-S}) + \int_{298}^{T_{lSc}} (C_{p,Fe} + C_{p,MnO} - C_{p,FeO} - C_{p,Mn}) dT \right) \quad \text{..... (41)}$$

$$\Delta H_{T-d}^\circ = \frac{x3_{d1}}{M_{Si}} \left((\Delta H_{SiO2} + \Delta H_{SiO2-S} - \Delta H_{FeO} - \Delta H_{Si-S}) + \int_{298}^{T_{lSc}} (2C_{p,Fe} + C_{p,SiO2} - 2C_{p,FeO} - 2C_{p,Si}) dT \right) \quad \text{..... (42)}$$

$$\Delta H_{T-e}^\circ = \frac{x5_{d1}}{M_{Cr}} \left((\Delta H_{Cr2O3} - 3\Delta H_{FeO} - \Delta H_{Cr-S}) + \int_{298}^{T_{lSc}} (3C_{p,Fe} + C_{p,Cr2O3} - 3C_{p,FeO} - 2C_{p,Cr}) dT \right) \quad \text{... (43)}$$

$$\Delta H_{T-f}^\circ = \frac{x6_{d1}}{M_P} \left((\Delta H_{P2O5} - 5\Delta H_{FeO} - 2\Delta H_{P-S}) + \int_{298}^{T_{lSc}} (5C_{p,Fe} + C_{p,P2O5} - 5C_{p,FeO} - 2C_{p,P}) dT \right) \quad \text{... (44)}$$

$$\Delta H_{T-g}^\circ = \frac{x2_{d2}}{M_C} \left((\Delta H_{CO} - \Delta H_{C-S}) + \int_{298}^{T_{lSc}} (C_{p,CO} - C_{p,C} - 0.5C_{p,O2}) dT \right) \quad \text{..... (45)}$$

$$if\ (r_P < 0)\ then\ \Delta H_{T-h}^\circ = \frac{x9d3 + x9d4}{M_{CO}} \left((\Delta H_{CO2} - \Delta H_{CO}) + \int_{298}^{T_{gas}} (C_{p,CO2} - C_{p,CO} - 0.5C_{p,O2}) dT \right)$$

$$if\ (r_P > 0)\ then\ \Delta H_{T-h}^\circ = \frac{x9d4}{M_{CO}} \left((\Delta H_{CO2} - \Delta H_{CO}) + \int_{298}^{T_{gas}} (C_{p,CO2} - C_{p,CO} - 0.5C_{p,O2}) dT \right) \quad \text{..... (46)}$$

$$\Delta H_{T-i}^\circ = \frac{x2_{d5}}{M_C} \left((\Delta H_{CO2} - \Delta H_{C-S}) + \int_{298}^{T_{lSc}} (C_{p,CO2} - C_{p,C} - C_{p,O2}) dT \right) \quad \text{..... (47)}$$

$$\Delta H_{T-j}^\circ = -\frac{x4_{d2}}{M_{Mn}} \left((\Delta H_{CO} + \Delta H_{Mn-S} - \Delta H_{MnO} - \Delta H_{C-S}) + \int_{298}^{T_{lSc}} (C_{p,Mn} + C_{p,CO} - C_{p,MnO} - C_{p,C}) dT \right) \quad \text{..... (48)}$$

$$\Delta H_{T-k}^\circ = \frac{x3_{d3}}{M_{Si}} \left((\Delta H_{SiO2} + \Delta H_{SiO2-S} - \Delta H_{MnO} - \Delta H_{Si-S}) + \int_{298}^{T_{lSc}} (2C_{p,Mn} + C_{p,SiO2} - 2C_{p,MnO} - C_{p,Si}) dT \right) \quad \text{.. (49)}$$

$$\Delta H_{T-l}^\circ = \frac{x3_{d2}}{M_{Si}} \left((\Delta H_{SiO2} + \Delta H_{SiO2-S} - \Delta H_{Si-S}) + \int_{298}^{T_{lSc}} (C_{p,SiO2} - C_{p,Si} - 2C_{p,O2}) dT \right) \quad \text{.... (50)}$$

$$\Delta H_{T-m}^\circ = \frac{x5_{d2}}{M_{Cr}} \left((\Delta H_{Cr2O3} - 2\Delta H_{Cr-S}) + \int_{298}^{T_{lSc}} (C_{p,Cr2O3} - 2C_{p,Cr} - 0.5C_{p,O2}) dT \right) \quad \text{..... (51)}$$

$$\Delta H_{T-n}^\circ = -\frac{CH4_{inj}}{M_{CH4}} \left((\Delta H_{CO2} + 2\Delta H_{H2O} - \Delta H_{CH4}) + \int_{298}^{T_{gas}} (C_{p,CO2} + 2C_{p,H2O} - C_{p,CH4} - 2C_{p,O2}) dT \right) \quad \text{..... (52)}$$

Besides the above chemical reactions, the model also con-

siders graphite (C) electrode oxidation and the burning of the combustible materials present in the solid scrap. The energies of the reactions can be represented by the Eqs. (53) and (54). The model assumes the electrode graphite oxidizes to CO_2. The burning of the combustible materials is approximated by oxidizing C_9H_{20} to CO_2 and H_2O:

$$\Delta H^{\circ}_{T-o} = -\frac{\dot{m}_{el}}{M_C}\left((\Delta H_{CO2}) + \int_{298}^{T_{gas}} (C_{p,CO2} - C_{p,C} - C_{p,O2})dT\right); \quad \text{..... (53)}$$

$$\Delta H^{\circ}_{T-p} = -\frac{\dot{m}_{comb}}{M_{C9H20}}\left((\Delta H_{CO2} + \Delta H_{H2O} - \Delta H_{C9H20}) + \int_{298}^{T_{gas}} (C_{p,CO2} + C_{p,H2O} - C_{p,C9H20} - C_{p,O2})dT\right); \quad \text{.... (54)}$$

The total energy of the chemical reactions for the liquid metal ($Q_{lSc\text{-}chem}$) and the CO post-combustion ($Q_{CO\text{-}post}$) zones, which are used in part 1 paper[(PART 1)] can be obtained with Eq. (55):

$$Q_{lSc-chem} = \sum_i \Delta H^{\circ}_{T-var_i} - H^{\circ}_{T-h} \; var_i = a,\ldots,p$$
$$Q_{CO-post} = \Delta H^{\circ}_{T-h} \quad \text{.... (55)}$$

2.5. Foaming Slag Height

Slag foaming represents an important part of the EAF steel-making processes, since it has several positive characteristics. The most important characteristic of the foaming slag is its ability to revert a great portion of the radiative energy dissipated from the electric arcs to the bath instead to the furnace roof and walls. In this way, greater input powers to the EAF can be achieved, since the radiative impact to the furnace lining is reduced. The other advantage of the foaming slag is that among others it captures the CO bubbles, which increases the CO post-combustion efficiency. Another advantage of the slag is also its influence on stabilizing the burning of the arcs and consequently reducing their chaotic behavior and lowering the arc impedance load. The slag-foaming index (Ξ) can be defined by Eq. (56):[4)]

$$\Xi = \frac{\eta^{1.2}}{\sigma^{0.2}\rho D_B^{0.9}}, \quad \text{..... (56)}$$

where η, σ and ρ represent the slag's viscosity, surface tension and density, respectively, while D_B represents the foam-bubble diameter, and these are obtainable from the equations proposed by Zhang and Frueham in Ref. 4). The change of slag height can be obtained from Eq. (57):

$$\dot{H}_f = \Xi V_g, \quad \text{..... (57)}$$

where Ξ is the slag index obtained from Eq. (56) and V_g is the superficial gas velocity obtained from Eq. (58):

$$V_g = \frac{(\frac{1}{M_{CO}} x9_{d2}) R_{gas} T_{gas}}{(r_P + a_P)\pi r_1^2}, \quad \text{..... (58)}$$

where $x9_{d2}$ is the CO produced from oxidation, R_{gas} is the universal gas constant, T_{gas} is the temperature of the gas obtainable from Eq. (37) in part 1[(PART 1)], r_P is the relative pressure in the furnace obtainable from Eq. (35), a_P is the atmospheric pressure, while πr_1^2 accounts for the cross-sectional area of the EAF.[10)]

The factor that determines the relation between the slag height and the corresponding view-factor change was modeled in a similar way to that proposed by MacRosty[3)] with the following Eq. (59):

$$K_{slag} = 0.7\left(\frac{1}{2}\tanh(5H_f - 1.25) + \frac{1}{2}\right)\left(\frac{1}{2}\tanh(3.2\left(1 - \frac{m_{sSc}}{m_{init}}\right) - 1.29) + \frac{1}{2}\right), \quad \text{..... (59)}$$

where H_f is the slag height, m_{sSc} is the mass of solid steel[(PART 1)] and m_{init} is the initial mass of the steel scrap loaded during each charge.

The factor ($1\text{-}K_{slag}$) is used to multiply the calculated view factors from arcs to roof ($VF_{5\text{-}1}$) and walls ($VF_{5\text{-}1}$)[(PART 1)], which models the decrease of the latter with the increasing slag height. Since the view factors from arc to solid ($VF_{5\text{-}3}$) and liquid ($VF_{5\text{-}4}$) metal are obtained from the reciprocity rule from $VF_{5\text{-}1}$ and $VF_{5\text{-}2}$, they increase with the increasing slag height accordingly.

3. Results and Discussion

The following section presents the simulation results that are relevant to the proposed thermo-chemical model and were obtained by combining the developed mathematical models for the mass and heat transfer and the chemical reactions. Some of the obtained results are compared with the available endpoint measurements, such as the composition of the steel and the slag. Other non-measured values are compared to the results of the studies, which address similar EAF topics.

3.1. Simulation Timeline

The following results were obtained using the same simulation timeline as presented in part 1 paper.[(PART 1)]

3.2. Initial Steel and Slag Composition

As is generally known, the initial composition of the steel scrap and the added slag-forming materials are crucial for obtaining the end-point compositions; therefore, the compositions used for the simulation are defined as in a real operation as follows:

- Steel composition: 0.4% C, 0.6% Si, 0.2% Cr, 0.05% P, 0.6% Mn and 1.1% combustibles,
- Slag composition: 56.7% CaO, 41.2% MgO, 0.7% SiO_2 and 0.45% Al_2O_3.

Also, an assumption is made that all the slag-forming material added during the melting process has the same chemical composition.

3.3. Thermo-chemical Model

Figure 1 shows the powers (left panel) and energies (right panel) of the chemical reactions occurring in the furnace.

P_{CH4} and Q_{CH4} represent the oxygen burners (Eqs. (1n) and (52)), $P_{electrodes}$ and $Q_{electrodes}$ represent the electrode oxidation (Eqs. (36) and (53)), $P_{combustible}$ and $Q_{combustible}$ represent the oxidation of combustible materials (Eqs. (37) and (54)), while $P_{chemical}$ and $Q_{chemical}$ represent the sum of all the chemical reactions described in section 2.1. It can be seen that the largest increase in the chemical power occurs after the O_2 stream is started (t = 1 000 s), which indicates the importance of O_2 lancing for an additional energy input and

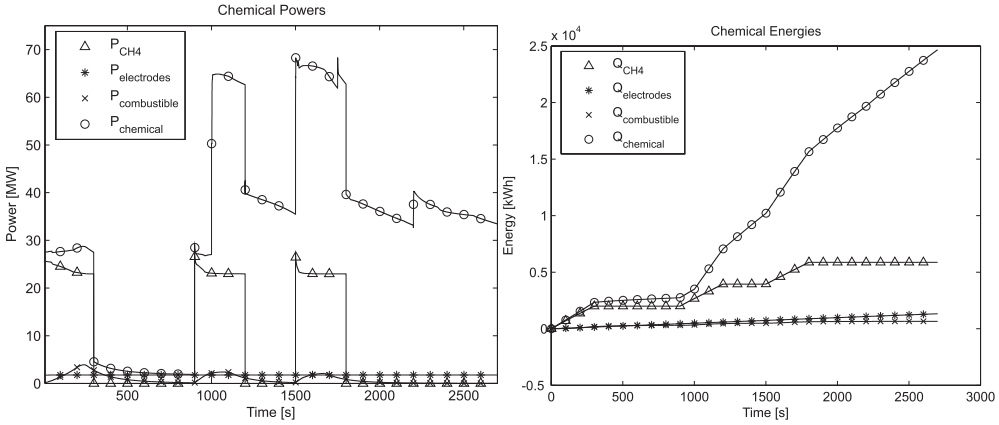

Fig. 1. Left panel: Power of chemical reactions; Right panel: energy of chemical reactions.

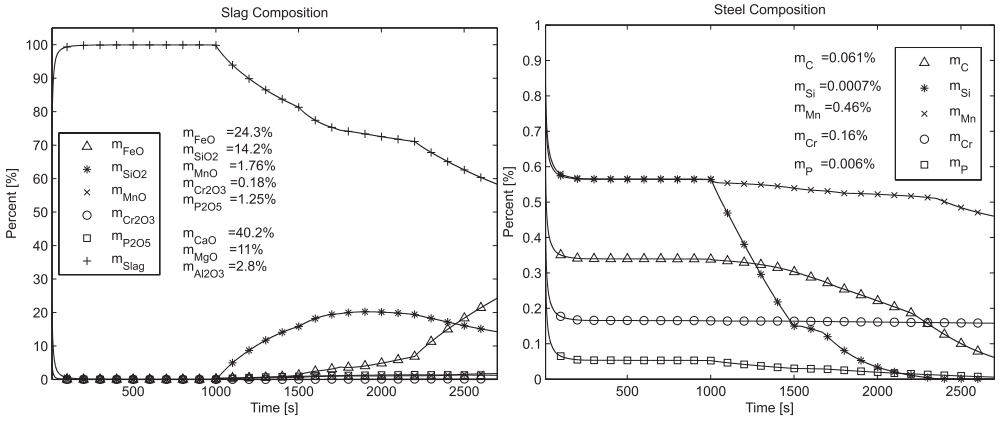

Fig. 2. Left panel: Slag composition - m_{slag}, marked with +, represents the sum of compounds CaO, MgO and Al_2O_3, m_{xx} denotes the endpoint percentage of a given compound in slag; Right panel: steel composition, m_{xx} denotes the endpoint percentage of a given element in steel bath.

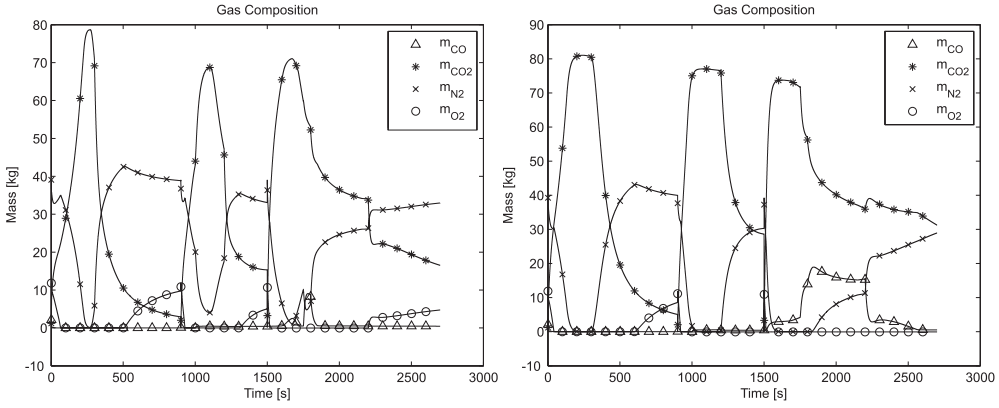

Fig. 3. Left panel: Gas composition with CO post-combustion; Right panel: Gas composition without CO post-combustion.

the endpoint composition of the slag and the steel.

Figure 2 shows the slag (left panel) and steel (right panel) compositions. With regard to the initial slag and steel compositions and the suggestions of other studies,[5,8] both compositions obtained with the proposed model are satisfactory. Like with the energy of the chemical reactions, the rate of change of an individual element or compound in the slag or steel is subject to O_2 (t = 1 000 s) and C injection, which further indicates the importance of the oxygen-lancing technology for the energy balance and the final composition of the steel.

Figure 3 shows the gas composition profiles when simulating the EAF model with (left panel) and without (right panel) CO post-combustion. It can be seen that in the case of CO post-combustion all the O_2 and CO are consumed. When an additional O_2 stream, used for the CO post-combustion is turned off, the amount of CO in the gas zone reaches up to 40%. Also observable, when charging baskets 1 and 2, is a rapid release of CO_2, which is a consequence of burning the combustible materials shortly after the steel is loaded and other oxidation reactions, which produce CO_2.

3.4. Model Validation

To further validate the developed EAF model and to

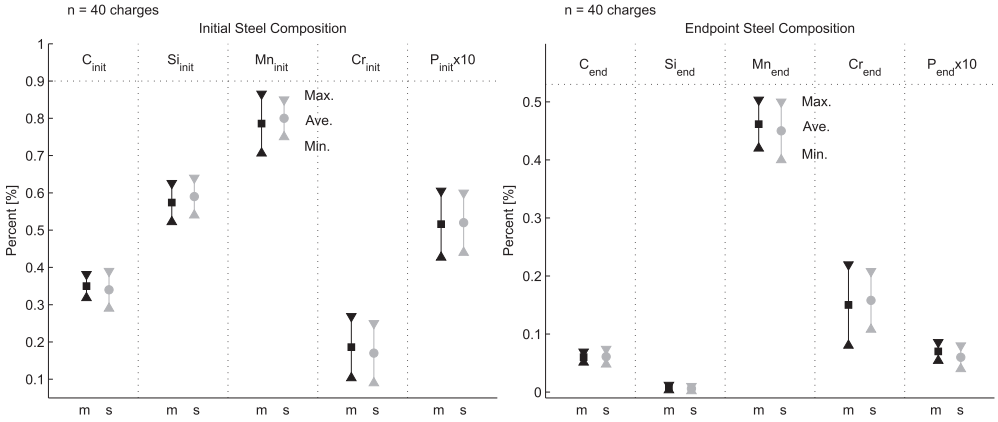

Fig. 4. Comparison between measured (m) and simulated (s) initial and endpoint steel composition values, indicating minimum (Min.), average (Ave.) and maximum (Max.) values.

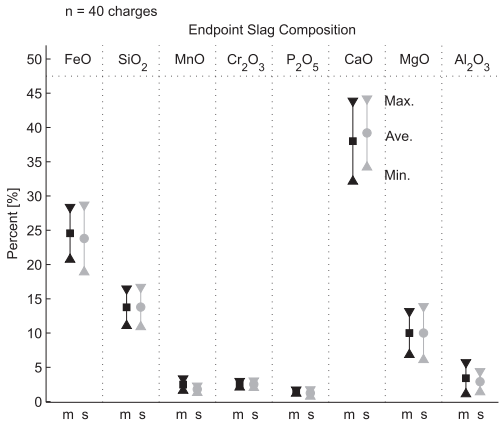

Fig. 5. Comparison between measured (m) and simulated (s) endpoint slag composition values, indicating minimum (Min.), average (Ave.) and maximum (Max.) values.

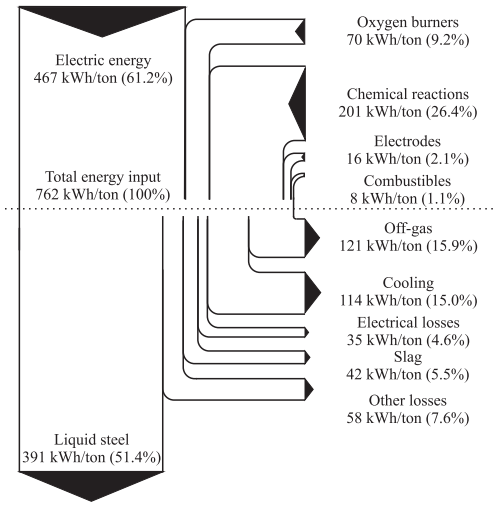

Fig. 6. Energy balance of the EAF obtained from the proposed models.

Table 1. Comparison between the initial and endpoint measured and simulated mean steel composition values, including standard deviations.

	C [%]	Si [%]	Mn [%]	Cr [%]	P [%]
Measured initial	0.35±0.031	0.57±0.052	0.79±0.079	0.19±0.082	0.05±0.009
Simulated initial	0.34±0.049	0.59±0.050	0.80±0.053	0.17±0.083	0.05±0.008
Measured endpoint	0.06±0.009	0.0078±0.0043	0.46±0.042	0.15±0.069	0.007±0.002
Simulated endpoint	0.061±0.013	0.0061±0.0041	0.45±0.047	0.16±0.049	0.006±0.003

Table 2. Comparison between the endpoint measured and simulated mean slag composition values, including standard deviations.

	FeO [%]	SiO_2 [%]	MnO [%]	Cr_2O_3 [%]	P_2O_5 [%]	CaO [%]	MgO [%]	Al_2O_3 [%]
Measured	24.6±3.8	13.7±2.7	2.5±0.9	2.5±0.4	1.5±0.3	38.0±5.9	10.0±3.2	3.4±2.3
Simulated	23.8±4.9	13.8±2.9	1.9±0.5	2.5±0.5	1.3±0.5	39.2±5.0	10.1±3.9	2.9±1.5

ensure its appropriateness for the initial aims of this study, the simulated initial and endpoint steel and slag compositions were compared to the measured operational data and are presented in **Figs. 4** and **5** and **Tables 1** and **2**. The measured average values were obtained from the data for 40 different heats, while the simulated values were obtained from the model using different initial conditions.

As can be seen in Figs. 4 and 5 and Tables 1 and 2, the measured and simulated endpoint data are similar, which indicates the accuracy of the proposed chemical model and its usability for further analysis, *i.e.*, the energy optimization and the operator-training simulator. Other values, important for the validation, such as: energy consumption, steel yield, temperatures and power-on-times, are given in part 1 paper(PART 1) or were already presented.[1)]

Figure 6 shows the energy balance of the particular EAF obtained from the proposed models. The total electric energy input and electric losses were obtained using an electrical model of the EAF,[1)] while other energies were obtained with the presented models.

It can be seen that total input and output energies of the EAF coincide with other similar EAF assemblies,[5)] which further proves the appropriateness of the developed EAF model. Energy from the chemical reactions accounts up to 25% of the total energy, which indicates that more C and O_2 could be added into the bath, to reduce electrical energy and achieve better energy balance.

4. Conclusion

In this paper an approach to the mathematical modeling and validation of thermo-chemical reactions for the EAF processes is presented. The proposed model covers the most common chemical processes and reactions and includes

some other important aspects, such as CO post-combustion, oxygen burners, electrode oxidation and other processes that are often neglected in the EAF modeling practice. The developed model could be extended with other reactions for the steel-melting process of lower importance; however, due to the lack of endpoint composition measurements which would include the percentages of the particular elements or compounds and a relative simplicity of the proposed model, the equations describing those reactions were omitted at this point. The obtained model is developed in accordance with the fundamental laws of thermo-chemistry. Parameterization of the model is carried out using available initial and end-point operational measurements, theoretical data and conclusions of different studies examining such processes in the EAF, as some of the parameters could not be obtained from the available operational data. Whether some additional measurements could be performed, better estimation of some parameters could be achieved. Even though, comparing the presented results to the available measurements, the proposed model can be considered as appropriate for the aims of the study, as high levels of similarity were achieved between the simulated results and both the theoretical and practical data available. By incorporating the thermo-chemical model into the already developed framework of electrical, hydraulic,[1] heat, mass and temperature models[(PART 1)] a complete EAF model is obtained, which shall further be used for operator training simulator and enhancement of the EAF process, in terms of energy and cost reduction/optimization.

Acknowledgement

The work presented in this paper was funded by Slovenian Research Agency (ARRS) project *J2-2310 Monitoring and Control of Steel Melt Quality in Electric Arc Furnace*.

REFERENCES

1) V. Logar, D. Dovžan and I. Škrjanc: *ISIJ Int.*, **51** (2011), No. 3, 382.
2) J. G. Bekker, I. K. Craig and P. C. Pistorius: *ISIJ Int.*, **39** (1999), No. 4, 23.
3) R. D. M. MacRosty and C. L. E. Swartz: *Ind. Eng. Chem. Res.*, **44** (2005), No. 21, 8067.
4) E. T. Turkdogan and R. J. Frueham: The Making, Shaping and Treating of Steel, 10th ed., Chapter 2: Fundamentals of Iron and Steelmaking, The AISE Steel Foundation, Pittsburgh, PA, USA, (1998), 13.
5) J. A. T. Jones, B. Bowman and P. A. Lefrank: The Making, Shaping and Treating of Steel; 10th ed., Chapter 10: Electric Furnace Steelmaking, The AISE Steel Foundation, Pittsburgh, PA, USA, (1998), 525.
6) M. Kirschen, V. Velikorodov and H. Pfeifer: *Energy*, **31** (2006), No. 14, 2926.
7) M. G. Grant: 58th Electric Furnace Conference, ISS, Warrendale, PA, USA, (2000), 15.
8) E. T. Turkdogan: Fundamentals of Steelmaking, Institute of Materials, London, UK, (1996).
9) S. Basu: PhD thesis, Royal Institute of Technology, Stockholm, Sweden, (2007).
10) D. J. Oosthuizen, J. H. Viljoen, I. K. Craig and P. C. Pistorius: *ISIJ Int.*, **41** (2001), No. 4, 399.
11) H. Sun: *ISIJ Int.*, **45** (2005), No. 10, 1482.
12) H. S. Kim, J. G. Kim and Y. Sasaki: *ISIJ Int.*, **50** (2010), No. 5, 678.
13) H. Sun, M. Y. Lone, S. Ganguly and O. Ostrovski: *ISIJ Int.*, **50** (2010), No. 5, 639.
14) Y. E. Lee, L. Kolbeinsen: *ISIJ Int.*, **45** (2005), No. 9, 1282.
15) S. Kitamura, K. Miyamoto, H. Shibata, N. Maruoka and M. Matsuo: *ISIJ Int.*, **49** (2009), No. 9, 1333.
16) W. Kurz and D. J. Fisher: Fundamentals of Solidification, Trans Tech Publications, Ltd., Switzerland, (2005).

Appendix

Table 3 gives the values of the reaction rates (kg/s) for the presented chemical reactions. The displayed rates are relatively approximate and rounded to a nearest integer, since minor deviations from the estimated rates do not significantly change the simulation results. Rate estimations can be obtained from different sources studying thermo-chemical processes. In this manner, $kd_{C\text{-}L}$ can be obtained from,[1] $kd_{C\text{-}D}$ and $kd_{Si\text{-}1}$ can be obtained from,[2,4] $kd_{C\text{-}1}$ and $kd_{C\text{-}2}$ can be obtained from,[4,12] $kd_{Mn\text{-}1}$ can be obtained from,[13] $kd_{Mn\text{-}2}$, $kd_{Si\text{-}2}$, $kd_{Cr\text{-}1}$ and $kd_{Cr\text{-}2}$ can be obtained from,[4] kd_{Mn} can be obtained from[14] and kd_P can be obtained from.[15]

Table 4 gives the values of enthalpies of formation used in Eqs. (39) to (54). All rates are in kJ/mol and can be obtained from.[4]

Table 5 gives the values of all other parameters used in the model including the units. Some parameters, such as: V_{gas}, R_{tip}, R_{side}, A_{side} and r_1 are EAF specific, k_{AIR1}, k_{AIR2}, k_{PR}, h_d, k_U and u_2 can be obtained from,[2] λ_C can be obtained from,[16] $K_{O2\text{-}CO}$, $K_{O2\text{-}CO2}$, $K_{O2\text{-}Cr2O3}$, $K_{O2\text{-}FeO}$, $K_{O2\text{-}SiO2}$, $K_{FeO\text{-}DRI}$, $K_{Fe\text{-}DRI}$ and kd_{comb} can be, with minor approximations, obtained from,[4,5,8] while R_{gas}, T_{melt} and a_P represent universal gas constant, steel melting point and atmospheric pressure.

Table 3. Reaction rates used in the model. All rates are in kg/s.

$kd_{C\text{-}L}$	$kd_{C\text{-}D}$	$kd_{C\text{-}1}$	$kd_{C\text{-}2}$	$kd_{Mn\text{-}1}$	$kd_{Mn\text{-}2}$
15	35	60	55	20	10
kd_{Mn}	$kd_{Si\text{-}1}$	$kd_{Si\text{-}2}$	$kd_{Cr\text{-}1}$	$kd_{Cr\text{-}2}$	kd_P
75	144	250	3	1	35

Table 4. Enthalpies of formation used in the model. All units are in kJ/mol.

ΔH_{FeO}	$\Delta H_{Fe\text{–}S}$	ΔH_{CO}	ΔH_{CO2}	$\Delta H_{C\text{–}S}$	$\Delta H_{Mn\text{–}S}$	ΔH_{MnO}	$\Delta H_{Si\text{–}S}$
–243	00	–117	–396	–27	–20	–385	–132
ΔH_{SiO2}	$\Delta H_{SiO2\text{–}S}$	$\Delta H_{Cr\text{–}S}$	ΔH_{Cr2O3}	$\Delta H_{P\text{–}S}$	ΔH_{P2O5}	ΔH_{H2O}	ΔH_{CH4}
–946	–45	–42	–1 142	–29	–2 940	–247	–91

Table 5. Values of other parameters used in the model.

λ_C	$K_{O2\text{-}CO}$	$K_{O2\text{-}CO2}$	$K_{O2\text{-}Cr2O3}$	$K_{O2\text{-}FeO}$	$K_{O2\text{-}SiO2}$	$K_{FeO\text{-}DRI}$	$K_{Fe\text{-}DRI}$
117 $\frac{\text{kJ}}{\text{mol}}$	0.05	0.15	0.015	0.75	0.035	0.07	0.93
k_{AIR1}	k_{AIR2}	k_{PR}	h_d	k_U	u_2	R_{gas}	V_{gas}
7.3 $\frac{\text{mol}}{\text{kg}}$	27.4 $\frac{\text{mol}}{\text{kg}}$	0.6	0.65	6.44	0.3 m	8.314 $\frac{\text{J}}{\text{molK}}$	45 m^3
R_{tip}	R_{side}	A_{side}	T_{melt}	a_P	r_1	kd_{comb}	u_1
0.02 $\frac{\text{kg}}{\text{kA hr}}$	10 $\frac{\text{kg}}{\text{m}^2\ \text{hr}}$	0.35 m^2	1 809 K	101.3 kPa	3.3 m^2	0.1 s^{-1}	15 kg/s